


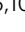





Ubiquitous karst hydrological control on speleothem oxygen isotope variability in a global study

Pauline C. Treble ^{1,2✉}, Andy Baker ^{1,2}, Nerilie J. Abram ^{3,4}, John C. Hellstrom⁵, Jagoda Crawford¹, Michael K. Gagan^{6,7}, Andrea Borsato ⁸, Alan D. Griffiths ¹, Petra Bajo^{1,5,10}, Monika Markowska^{1,11}, Stacey C. Priestley ^{1,12}, Stuart Hankin¹ & David Paterson ⁹

Speleothem oxygen isotopic ($\delta^{18}\text{O}$) records are used to reconstruct past hydroclimate yet records from the same cave do not always replicate. We use a global database of speleothem $\delta^{18}\text{O}$ to quantify the replicability of records to show that disagreement is common worldwide, occurs across timescales and is unrelated to climate, depth or lithology. Our global analysis demonstrates that within-cave differences in mean speleothem $\delta^{18}\text{O}$ values are consistent with those of dripwater, supporting a ubiquitous influence of flowpaths. We present a case study of four new stalagmite records from Golgotha Cave, southwest Australia, where the isotopic differences between them are informed by cave monitoring. It is demonstrated that karst hydrology is a major driver of within-cave speleothem and dripwater $\delta^{18}\text{O}$ variability, primarily due to the influence of fractures on flowpaths. Applying our understanding of water movement through fractures assists in quantitative reconstruction of past climate variability from speleothem $\delta^{18}\text{O}$ records.

¹ ANSTO, Lucas Heights, Australia. ² School of Biological, Earth and Environmental Sciences, UNSW Sydney, Kensington, Australia. ³ Research School of Earth Sciences, Australian National University, Canberra, Australia. ⁴ ARC Centre of Excellence for Climate Extremes, Australian National University, Canberra, Australia. ⁵ School of Geography, Earth and Atmospheric Sciences, University of Melbourne, Parkville, Australia. ⁶ School of Earth, Atmospheric and Life Sciences, University of Wollongong, Wollongong, Australia. ⁷ School of Earth and Environmental Sciences, The University of Queensland, St Lucia, Australia. ⁸ School of Environmental and Life Sciences, University of Newcastle, Callaghan, Australia. ⁹ Australian Synchrotron ANSTO, Clayton, Australia. ¹⁰ Present address: Croatian Geological Survey, Zagreb, Croatia. ¹¹ Present address: Max Planck Institute for Chemistry, Mainz, Germany. ¹² Present address: School of Physical Sciences, University of Adelaide, Adelaide, Australia. ✉email: pauline.treble@ansto.gov.au

Oxygen isotopes are a well-studied tracer of water and thus the hydrological cycle^{1–3}. Preservation of O isotopes within paleoenvironmental archives provides an opportunity to study past hydroclimatic variability⁴ as well as climate dynamics with external forcing different to the present^{5,6}. Speleothems are excellent paleoclimate archives as they can provide continuous, high resolution $\delta^{18}\text{O}$ records with well-constrained chronologies and they occur over most climatic zones where limestone karst exists (e.g., see refs. 7,8). These properties have motivated the collation of speleothem $\delta^{18}\text{O}$ records into global databases^{9–11} that facilitate regional synthesis of these data to identify past climate patterns;¹² and promote data-model comparisons to evaluate the performance of climate models across different past climate states¹³.

Measurement of speleothem $\delta^{18}\text{O}$ is routine, and these values reflect the isotopic composition of source water (meteoric precipitation) and cave temperature¹⁴. However, speleothem $\delta^{18}\text{O}$ may not always be an ideal proxy for hydroclimate owing to variable karst flowpaths between water falling as meteoric precipitation and emerging as dripwater within a cave¹⁵. Additional processes can also influence the fractionation of $^{18}\text{O}/^{16}\text{O}$ between dripwater and calcite¹⁴. In the quest to reach quantitative reconstruction of climate variability from speleothem $\delta^{18}\text{O}$, increasing attention has been focused on constraining the latter^{16–19} while the impact of flowpaths (karst store volume, infiltration thresholds, matrix versus fracture flow type) is less widely acknowledged. Some studies have utilised karst hydrology models to simulate the potential for the physical characteristics of flowpaths to impact dripwater $\delta^{18}\text{O}$ ^{20,21}; but validation of the impact of these processes on the speleothem record is limited by the relatively few studies where speleothem $\delta^{18}\text{O}$ has been accompanied by cave monitoring^{22–27}.

The recognised complexities of speleothem $\delta^{18}\text{O}$ means that replication of speleothem records from the same cave or karst region is considered the gold standard in assessing their robustness as paleo-environmental archives^{12,28}. Yet coeval records from the same cave frequently do not replicate in detail—often displaying differences in mean, variability and trends (e.g., see refs. 29,30). Studies using coeval records commonly create merged datasets, termed master or composite records, by splicing techniques that scale records according to mean values^{31,32} or apply a filter through merged datasets^{33,34}. The application of largely arbitrary data corrections may result in loss of information, including the statistical mean $\delta^{18}\text{O}$ value that is a critical target for model performance (e.g., see ref. 35), as well as the loss of opportunity for further quantification of hydroclimatic information if a more mechanistic understanding of flowpaths was applied³⁶.

Here, we quantify the within-cave differences in mean $\delta^{18}\text{O}$ values using global compilations of speleothem and dripwater data. For speleothems, we used the SISALv2 database¹¹ to identify caves with multiple coeval speleothem $\delta^{18}\text{O}$ records, and for dripwater we enlarge the global dataset of ref. 37 from 39 to 50 caves using expanded criteria (see “Methods” section). We then improve our understanding of the processes giving rise to different mean values for dripwater $\delta^{18}\text{O}$ between flowpaths through a case study of coeval speleothem records from Golgotha Cave (southwest Australia; Fig. 1). Uniquely, within the Golgotha Cave system, dripwater hydrochemistry is well-constrained by long-term monitoring³⁸ and individual flowpaths have been characterised by a spatially dense array of 34 automated drip loggers and lidar mapping^{39–41}. This setting allows us to, for the first-time, robustly assess the role that karst hydrology plays in determining the $\delta^{18}\text{O}$ variability between coeval speleothem paleoclimate records.

Results and discussion

Global speleothem and drip $\delta^{18}\text{O}$ assessment. A collation of dripwater and speleothem mean $\delta^{18}\text{O}$ values was prepared for 50 caves with 229 drip monitoring sites, and 64 caves with 146 pairs of coeval speleothem records (Fig. 1; and Supplementary Table 1, Supplementary Data 1, 2 and 3; see “Methods” section). For speleothems we calculate the difference in mean $\delta^{18}\text{O}$ values ($\Delta\delta^{18}\text{O}_{\text{means}}$) between paired coeval records and for dripwater we calculate the range in dripwater mean $\delta^{18}\text{O}$ values. We find that within-cave range of dripwater mean $\delta^{18}\text{O}$ values is greater than $>0.3\text{‰}$ for 52% of caves; and 45% of coeval speleothem pairs had a difference in mean $\delta^{18}\text{O}$ values ($\Delta\delta^{18}\text{O}_{\text{means}}$) $>0.3\text{‰}$. Analytical uncertainty is set at 0.3‰ based on inter-laboratory comparisons^{42,43}; as each coeval dataset will likely come from an individual laboratory where routine reproducibility can be several times better (e.g., typically 0.05‰ —see “Methods” section), our threshold for analytical uncertainty is very conservative and implies that our calculations represent the minimum percentage of caves demonstrating within-cave differences in mean $\delta^{18}\text{O}$ values.

Our findings demonstrate that within-cave variability in mean $\delta^{18}\text{O}$ values is common worldwide for both dripwater and speleothem data. The global average for the within-cave range in dripwater mean $\delta^{18}\text{O}$ values is $0.51\text{‰}_{\text{VSMOW}}$ and the global average speleothem $\Delta\delta^{18}\text{O}_{\text{means}}$ is $0.37\text{‰}_{\text{VPDB}}$ (Fig. 2). This implies that the majority of the within-cave differences in mean $\delta^{18}\text{O}$ values between coeval speleothem records may be inherited from the dripwater $\delta^{18}\text{O}$ and thus attributed to differences in karst flowpath physical properties.

Our analysis of the SISALv2 data utilised coeval speleothem records from all timescales including shorter, more finely resolved (annual to sub-decadal) records of the Holocene as well as longer records that span glacial–interglacial transitions. Dividing the data into two subsets representing speleothem records from the Holocene versus the Pleistocene epochs (Fig. 2), we show that the global average for either subset was not significantly different from the full dataset: p -value 0.29 (Holocene), p -value 0.20 (Pleistocene); one-tail distribution. The global average value of $\Delta\delta^{18}\text{O}_{\text{means}}$ was 0.34‰ for the Holocene (95 coeval speleothem pairs; 41% were $>0.3\text{‰}$) and 0.41‰ for the Pleistocene (51 pairs; 51% were $>0.3\text{‰}$) (Fig. 2). This demonstrates that within-cave differences in mean $\delta^{18}\text{O}$ values of coeval speleothems is common and similar in magnitude for both time periods, regardless of whether they are characterised by climate stability or instability.

The meta-data available with these global datasets allows us to further demonstrate that within-cave variability in mean $\delta^{18}\text{O}$ values in dripwater or coeval speleothems is not controlled by alternative factors such as site climate, cave depth or host rock geology. Cross-plots of within-cave variability in mean $\delta^{18}\text{O}$ values versus precipitation, temperature, aridity index, seasonality, latitude and elevation show weak to no relationships supported by negligible to low Kendall’s tau values (Fig. 3). Multiple linear regression (MLR) models were calculated and indicate that these factors explain only 14% or less of the within-cave variability in mean $\delta^{18}\text{O}$ values, whether dripwater or speleothem datasets were considered (Supplementary Table 2). Mann–Whitney U -tests using lithology as a factor showed no significant differences in mean values for different host rock types for either the dripwater or speleothem datasets (p -value = 0.05; Supplementary Fig. 1). We further investigate the possibility that within-cave differences in speleothem mean $\delta^{18}\text{O}$ values arises from isotopic fractionation processes during calcite precipitation driven by cave microclimate instability, by assessing the distance from the cave entrance to the speleothem locations (Fig. 3) but a low Kendall’s tau value (-0.17) shows no clear relationship. Thus

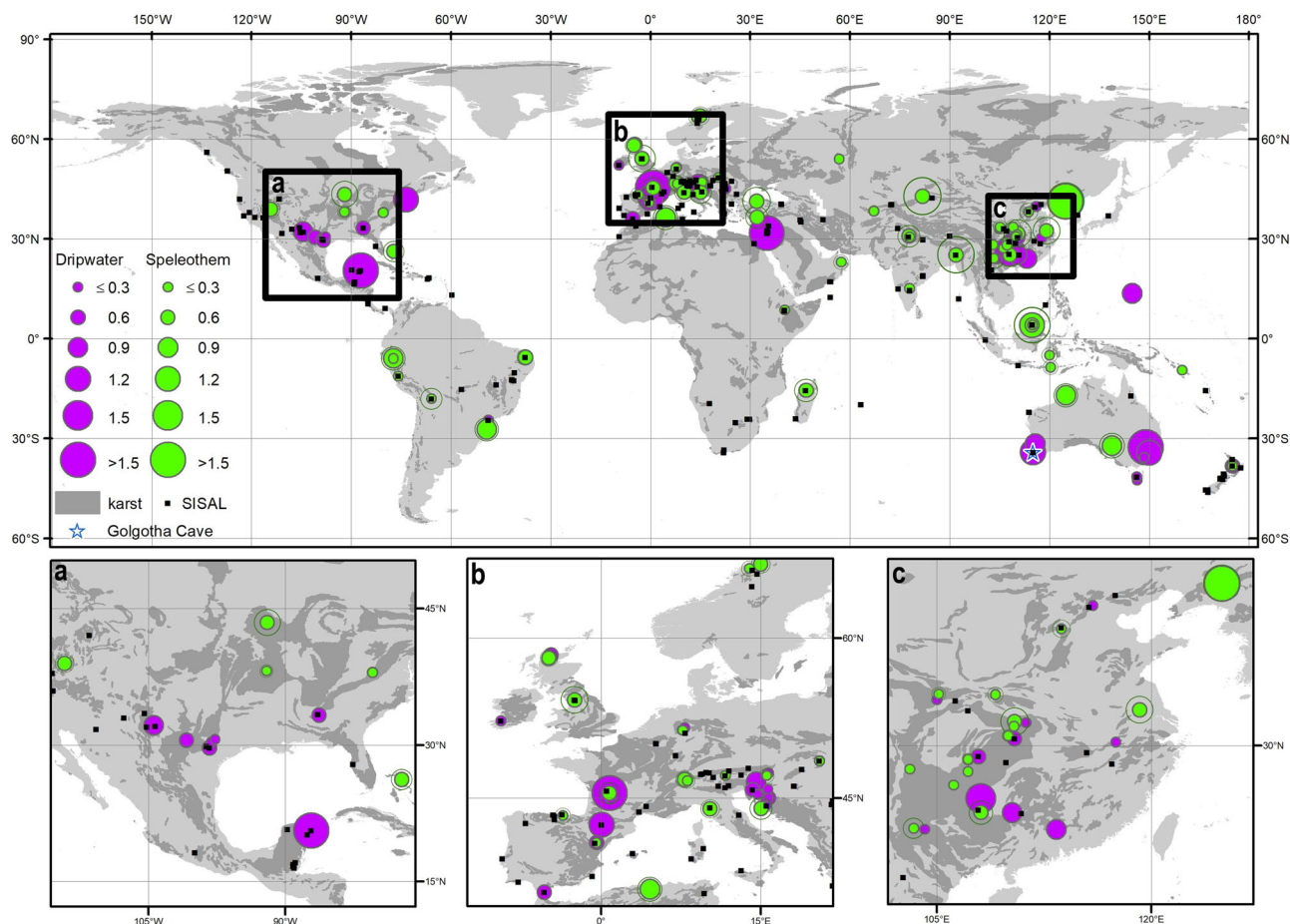


Fig. 1 Locations of caves and mean differences used in global meta-analysis of dripwater and speleothem datasets. The range of mean dripwater $\delta^{18}\text{O}$ values (purple) and the difference between mean values of coeval speleothem records ($\Delta\delta^{18}\text{O}_{\text{means}}$) (green) are indicated by symbol size for each cave. For caves with more than one set of coeval speleothem records the filled circle is the average value and the open circle is the maximum value of $\Delta\delta^{18}\text{O}_{\text{means}}$. Location of Golgotha Cave and other sites from the SISALv2 database are also shown. Darker grey shading indicates karst regions⁷⁰.

our global meta-analysis demonstrates that climate, geography, lithology or cave microclimate instability do not account for the ubiquitous within-cave variability in mean speleothem $\delta^{18}\text{O}$. Our meta-analysis further supports that flowpaths are responsible for the within-cave difference in coeval speleothem mean $\delta^{18}\text{O}$ values.

The global mean value for the within-cave difference in mean $\delta^{18}\text{O}$ values of coeval speleothems, $\Delta\delta^{18}\text{O}_{\text{means}}$, of $0.37\text{‰}_{\text{VPDB}}$ for speleothems is large and is exceeded for 51 caves in our analysis. Seven caves have coeval speleothem records with a difference in mean $\delta^{18}\text{O}$ values exceeding 1‰ (Supplementary Data 3), equivalent to one-third of glacial–interglacial cycles reproduced in stalagmites from the Asian monsoon region⁷. Thus, there is a need to further explore the role of flowpaths as the underlying mechanism for driving within-cave variability in mean speleothem $\delta^{18}\text{O}$ values. Just four caves in our global analysis have both dripwater and speleothem datasets^{29,44–50} and only one cave (NW Scotland^{45,46}; Fig. 1) has differences in mean $\delta^{18}\text{O}$ values for both drip and speleothem datasets. This highlights the need for more coeval speleothem datasets from monitored caves in order to objectively quantify the karst hydrological control on speleothem $\delta^{18}\text{O}$ variability.

Golgotha Cave case study. To address the above, we present a case study of four new stalagmite records that grew during the last eight centuries from Golgotha Cave, southwest Australia (Figs. 1 and 4a; see Supplementary Fig. 2 and ref. ³⁸ for site

description). Dripwater monitoring commenced after each stalagmite was removed and varies in length from 5 to 14 years duration (Figs. 4b and 5). Golgotha Cave represents a long and extensively characterised monitoring dataset^{38–41,51,52} to interrogate the influence of within-cave differences in karst flowpaths on speleothem $\delta^{18}\text{O}$ records. Cave temperature can be expected to have remained relatively constant over the period investigated eliminating the need to consider this variable.

Calcites farmed during our monitoring study permit an assessment of the reliability of Golgotha Cave speleothems to record changes in dripwater $\delta^{18}\text{O}$. In addition to the well-known potential complications of disequilibrium and/or kinetic effects⁵³, a recent study (ref. ¹⁹) hypothesised that in specific circumstances, speleothem $\delta^{18}\text{O}$ may be impacted by a process known as prior-calcite precipitation (PCP), a term commonly used for the calcite lost from solution along the flowpath prior to reaching the stalagmite⁵⁴. Ref. ¹⁹ utilised laboratory and modelling studies to interpret the $\delta^{18}\text{O}$ of calcite which was precipitated by solution flowing on an inclined slope at a flow rate such that oxygen isotope disequilibrium between HCO_3^- and H_2O occurred. For Golgotha Cave, empirical fractionation factors are calculated from in situ farmed calcites and dripwater to objectively constrain whether disequilibrium and/or kinetic effects, including PCP, are impacting the Golgotha Cave stalagmite $\delta^{18}\text{O}$ records (Table 1). The fractionation factors are consistent across the four speleothem sites in Golgotha Cave ($\alpha_{\text{calcite-water}} = 1.03185 \pm 0.00013$, $n = 9$; Table 1). If other effects, including PCP, dominated at the time of calcite

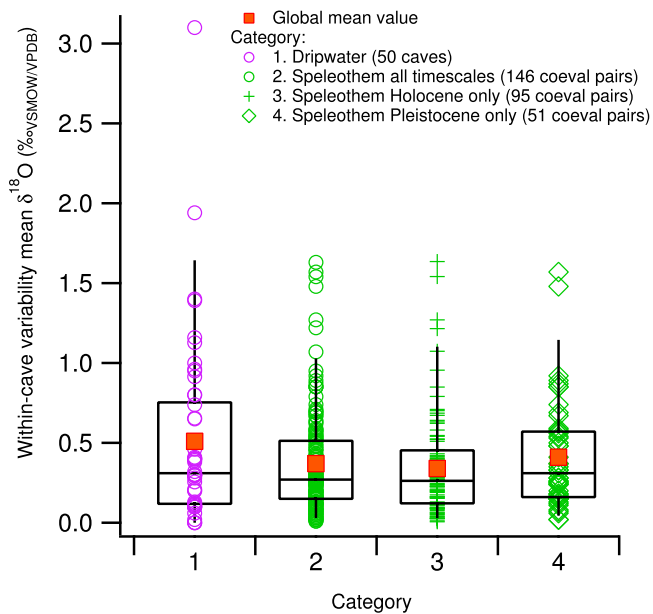


Fig. 2 Box and whisker plot comparing within-cave variability in dripwater and speleothem mean $\delta^{18}\text{O}$ values. The analysis demonstrates that within-cave variability in speleothem mean $\delta^{18}\text{O}$ values are comparable to the within-cave variability of dripwater mean $\delta^{18}\text{O}$ values, inferring a flowpath control. Category 1 (purple circles) are the range of dripwater mean $\delta^{18}\text{O}$ values for each cave and category 2 (green circles) are speleothem $\Delta\delta^{18}\text{O}_{\text{means}}$ for each pair of coeval records. Speleothem $\Delta\delta^{18}\text{O}_{\text{means}}$ are divided into Holocene (category 3, green crosses) and Pleistocene epochs (category 4; green diamonds). Orange squares indicate the mean value, boxes indicate the inter-quartile range and whiskers the 5th and 95th percentiles. Data from the global meta-analysis of dripwater and speleothem datasets.

precipitation, this would manifest as different $\alpha_{\text{calcite-water}}$ values between drip sites. The range of $1000\ln\alpha_{\text{calcite-water}}$ values is 0.3‰ which may be an indication of the magnitude of disequilibrium/kinetic/PCP effects, or measurement uncertainty. Regardless, a value of 0.3‰ is much smaller than the isotopic range in recent speleothem $\delta^{18}\text{O}$ values ($0.8\text{‰}_{\text{VPDB}}$) between sites (Fig. 4b; see Supplementary Notes 1–3 for further information on the robustness of these records).

Annual dripwater $\delta^{18}\text{O}$ mean values differ by up to 1‰_{VSMOW} between monitoring sites within Golgotha Cave³⁷ (Fig. 4b). Conversion of dripwater $\delta^{18}\text{O}$ to calcite equivalent values, using our farmed calcites, demonstrates that dripwater $\delta^{18}\text{O}$ gives a viable extension of the individual speleothem records associated with each drip (Fig. 4b). The difference in $\delta^{18}\text{O}$ values between flowpaths in the monitoring data are consistent with the isotopic offsets between speleothem records further confirming that the speleothem $\delta^{18}\text{O}$ records are primarily driven by differences in dripwater $\delta^{18}\text{O}$ values. The isotopic differences between the four speleothems persist throughout the 800 years of coeval data (Fig. 4a), but with differences in temporal evolutions of individual records that in the absence of consideration of karst processes could otherwise be misinterpreted to represent very different hydroclimate histories.

Variability in mean dripwater $\delta^{18}\text{O}$ associated with recharge thresholds and karst store behaviour can account for the differences observed in the $\delta^{18}\text{O}$ values of coeval speleothems within Golgotha Cave. We demonstrate this by drawing on our longitudinal monitoring data, updated with new data since ref. 38 and with dripwater sampling from new sites in our large drip logger array (Fig. 5). The majority of water movement to the

ceiling of Golgotha Cave is via flow through the matrix of the host-rock⁴¹ and is characterised by low drip rates with low variability^{38,40}. A second flow type, fracture flow, displays a threshold increase in drip rate in response to activation of flow along a fracture⁴⁰, while a third flow type termed combination flow has flow through an interconnected network of fractures and fissures/conduits⁴¹. Drips feeding the stalagmites in this study represent this range of flow types: predominately matrix (GL-S1, GL-S2), matrix plus fracture (GL-S4) and combination flow (GL-S3; Fig. 5b).

Fracture flow dripwaters have lower $\delta^{18}\text{O}$ values compared with matrix flow dripwaters and the isotopic value of fracture flowpaths is lower as the degree of fracture flow increases (Fig. 5c). Dripwater sampling from the additional sites in the drip logger array confirms that there is an isotopic distinction between matrix flow ($-4.0 \pm 0.1\text{‰}$, 1σ ; $n=58$) versus fracture flow ($-4.7 \pm 0.1\text{‰}$, $n=22$) classified drips⁴⁰ (Fig. 5c and Supplementary Data 4). Importantly, matrix flow is similar in value to precipitation-weighted monthly rainfall $\delta^{18}\text{O}$ (-3.9‰ ; Fig. 5c), indicating that matrix flow integrates the majority of rainfall events, whereas the lower $\delta^{18}\text{O}$ values of fracture flow drips (Fig. 5c) indicate that supply to fractures is biased towards larger rainfall events, which have relatively lower $\delta^{18}\text{O}$ values owing to the amount effect in this region^{52,55}. This recharge bias indicates that a threshold in rainfall intensity is required for flow along fractures to occur⁵⁶, consistent with studies elsewhere³⁷.

A fracture activation episode is evident in our dripwater monitoring data as an abrupt 115% increase in drip rate during November 2013 (GL-S4 drip; Fig. 5a, b). This occurred in response to a wetter than usual rainfall season (annual total above the 90th percentile) and is consistent with rapid, deep delivery of infiltrating rainwater along a fracture^{40,56}. The increase in flow was accompanied by a $0.5\text{‰}_{\text{VSMOW}}$ decrease in GL-S4 dripwater sustained for several years (Fig. 5c). The drip monitoring suggests that the relative volume of water contributed by large rainfall events to karst reservoirs is amplified by fractures and is related to the size and/or number of contributing fractures. The drip rate response for the combination flowpath (GL-S3) similarly rises in 2013 (Fig. 5b), only here the larger network of permeable features⁴⁰ smooths the response to infiltration. Dripwater $\delta^{18}\text{O}$ values for this site are the lowest of the four monitored sites, are 1‰_{VSMOW} lower than precipitation-weighted rainfall $\delta^{18}\text{O}$ and display low variability (Fig. 5c), consistent with the karst store for GL-S3 being sustained largely by infiltration via fractures.

The monitoring and characterisation of the Golgotha Cave system allows us to interpret the differences between the mean values of Golgotha Cave $\delta^{18}\text{O}$ speleothem records as well as the drivers of the variability through time. Records GL-S1 and GL-S4 have similar isotopic trends on multi-decadal to multi-centennial scales over the last eight centuries; however, the mean $\delta^{18}\text{O}$ value for GL-S4 is 0.5‰ lower (Fig. 4a). This is consistent with our identification of GL-S4 as receiving a larger component of fracture flow whilst GL-S1 is supplied predominately by matrix flow. Oxygen isotopic values for stalagmite GL-S1 do not fall below $-4.6\text{‰}_{\text{VPDB}}$, whereas they are typically below this value for GL-S4 (Fig. 4b). This indicates that selective recharge due to fracture activation during periods of higher rainfall was a persistent process impacting the flow pathway, hence the $\delta^{18}\text{O}$ record, of GL-S4. Further support for this process-based understanding is the typical widening of the isotopic offset between the two records that is observed during periods of relatively lower $\delta^{18}\text{O}$ values, e.g., 1250–1400 CE and 1580–1700 CE (Fig. 4a), indicative of enhanced fracture activation feeding GL-S4 in response to more intense rainfall events.

Additionally, from 1970 CE onwards, all records and their extended dripwater time series display rising $\delta^{18}\text{O}$ trends

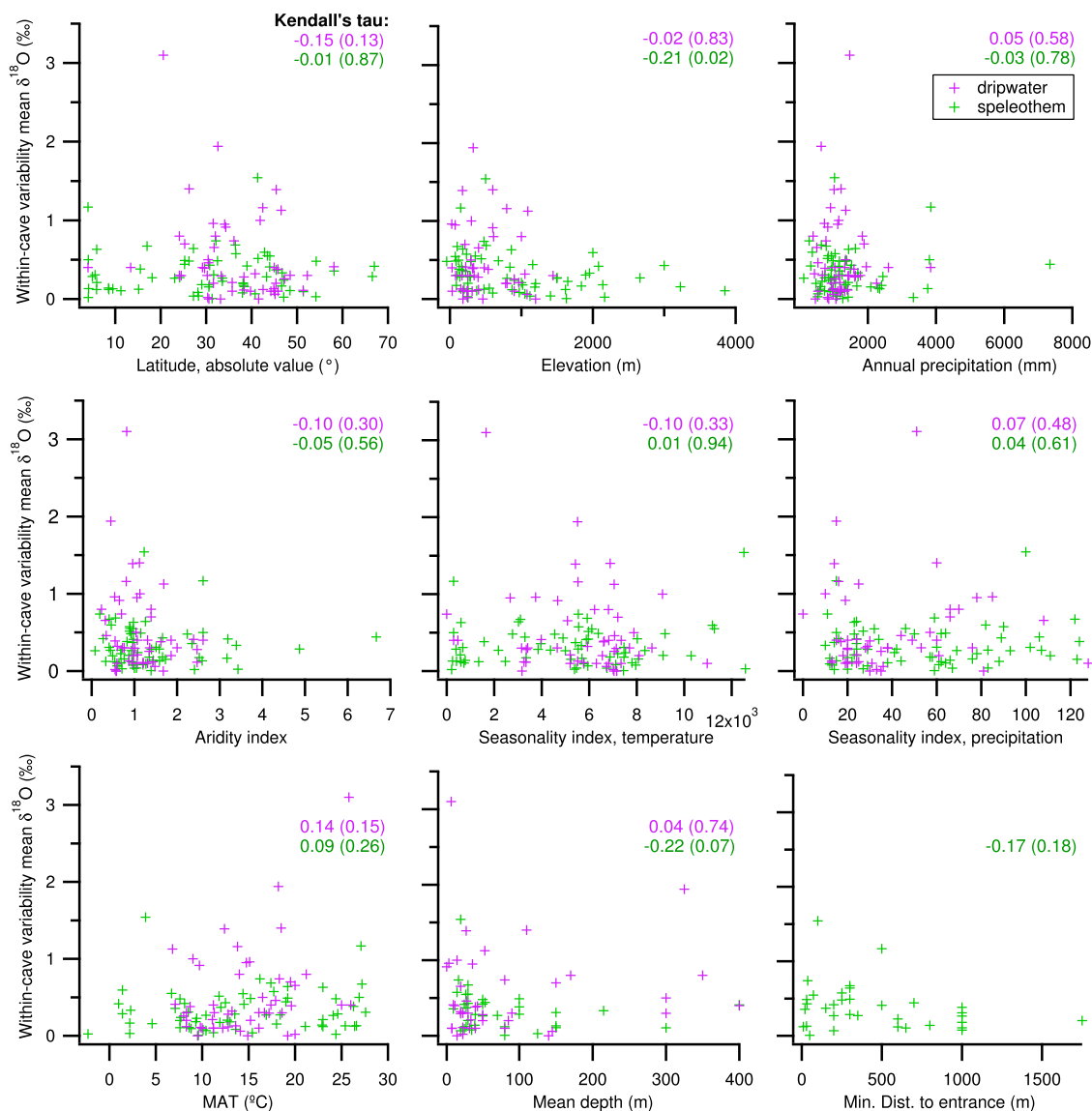


Fig. 3 Cross-plots of within-cave variability in dripwater and speleothem mean $\delta^{18}\text{O}$ values with climate and cave data. Cross-plots show low to no relationships between within-cave differences in dripwater (purple) or speleothem (green) mean $\delta^{18}\text{O}$ values with variables: latitude, elevation, annual precipitation, aridity index, seasonality indices for precipitation and temperature, mean annual temperature, mean depth, and minimum distance from entrance for each cave. The lack of relationship with these variables, demonstrated also by the output from the multiple linear regression models in Supplementary Table 2, supports that karst hydrological heterogeneity is important over all climate types, cave depths and host rock types. Kendall's tau values for each variable ranked against coeval dripwater and speleothem data are also shown, with p -values indicated in brackets. The p -values indicate that none of the relationships in are significant with the exception of elevation (SISAL; 95%) and mean depth (SISAL; 90%) although the Kendall's tau values are low. Aridity and seasonality indices are dimensionless.

coinciding with the sustained rainfall decrease in this region⁵⁷. We quantify the associated change in rainfall $\delta^{18}\text{O}$ to be $0.17\text{‰}_{\text{VSMOW}}$ by applying the empirically-derived relationship between rainfall $\delta^{18}\text{O}$ and amount for southwest Australia of ref. 52. The much larger $>1\text{‰}$ shift in the cave data demonstrates an additional mechanism is amplifying the isotopic response to climatic forcing and is consistent with a reduction in fracture flow, i.e., conditions were insufficient to overcome recharge threshold(s) for regular fracture activation⁵⁶ resulting in a isotopic shift towards the matrix-flow end-member. This clearly demonstrates how flowpath characteristics (threshold for activation and fracture contribution) amplify the response of dripwater $\delta^{18}\text{O}$ values to hydroclimate forcing.

Stalagmite GL-S2 $\delta^{18}\text{O}$ values are initially similar to GL-S4 from 1330 to 1440 CE, intermittent between GL-S1 and GL-S4

until 1560 CE, then at or above GL-S1 for the remainder of the speleothem and dripwater record (Fig. 4a, b). Temporal flow-switching was documented previously for GL-S2's drip site³⁸ and is consistent with its location in the cave characterised by our lidar-based study as having high-spatial heterogeneity in flow regime⁴⁰. In contrast, stalagmites GL-S1 and GL-S4 come from a section of the cave with low spatial variability in flow-paths attributed to their connectedness to the common hydrological domain of the matrix^{39,40}.

Fracture dominated flowpaths. Speleothems from drips that are dominated by combination or complex fracture flowpaths in Golgotha Cave show greater isotopic variability and less reliable growth consistent with their drip supplied by flow along fractures rather than through the matrix. Speleothem GL-S3 experienced

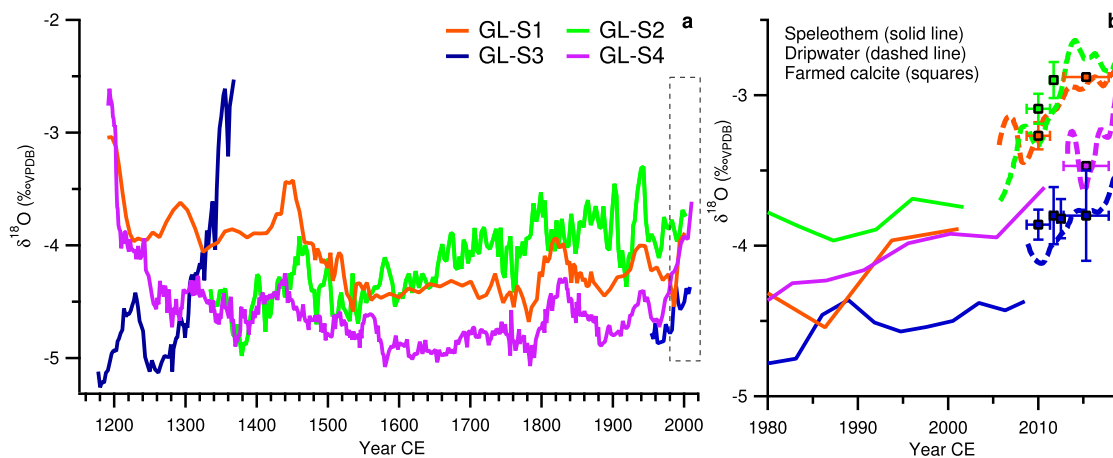


Fig. 4 Golgotha Cave speleothem $\delta^{18}\text{O}$ records. **a** Speleothem records GL-S1 (red), GL-S2 (green), GL-S3 (navy blue) and GL-S4 (purple) for the last 800 years. **b** Comparison between speleothem (solid line), dripwater (dashed line) and farmed calcite (squares) for the last four decades. Dashed box in **a** indicates region re-plotted in **b**. Dripwaters were converted to calcite equivalent values using an empirical bulk fractionation factor derived from calcites farmed at the drip sites (Supplementary Note 1 and Table 1). Dripwater (calcite equivalent $\delta^{18}\text{O}$ values) are used to extend the speleothem time series. The agreement (allowing for the rising trend) also supports the empirical fractionation factor calculated from Golgotha farmed calcites and dripwaters.

discontinuous growth over the last 800 years (Fig. 4a), with rejuvenation of growth commencing with low $\delta^{18}\text{O}$ values (e.g., 1180–1300 and again in the 1950s CE; Fig. 4a). This is consistent with flow to this speleothem dominated by fracture flowpaths⁴⁰ with a higher recharge threshold requiring relatively high infiltration from larger rainfall events to activate⁵⁶. For example, a relatively wet interval during the 13th century is supported by falling $\delta^{18}\text{O}$ values supplied by the matrix to GL-S1 plus fracture activation initiating growth to stalagmites GL-S2 and GL-S4. The higher recharge threshold for GL-S3's flowpath is evidenced by the $\delta^{18}\text{O}$ values that are up to 1 ‰_{VPDB} lower than the other records at 1200–1300 CE.

An enhanced non-linear response to recharge is also evident in GL-S3 shown by the rising trend that is initially similar in value to GL-S4 at 1300 CE after which, GL-S3 $\delta^{18}\text{O}$ values rise steeply by 1.5 ‰ in less than three decades, exceeding the matrix-flow record (GL-S1; Fig. 4a). The continuity of all the other records at the time when GL-S3 ceases growing (approx. 1380 CE) indicates that infiltration to the cave system is still occurring but not to the fractures supplying GL-S3, i.e., a stranded reservoir. The fact that both GL-S2 and GL-S4 $\delta^{18}\text{O}$ values are falling together (below matrix flow values) indicates that fractures are still supplying water elsewhere in the cave. The lack of supply to GL-S3 indicates flow-switching in a large complex fracture network with insufficient supplementation of flow from the matrix. The isotopic maximum prior to termination of the first growth phase in GL-S3: -2.5‰ (Fig. 4a) is similar to observed dripwater maxima ($\delta^{18}\text{O}$, calcite-equivalent; Fig. 4b), thus demonstrating that it could have been inherited from the dripwater, although additional processes may have also contributed as the amount of water feeding GL-S3 became increasingly diminished, including enhanced isotopic disequilibrium effects as the drip interval lengthens⁵⁸.

Speleothems associated with large, complex fractures are more likely to show non-linear responses to hydroclimate forcing and more caution should be taken with interpreting paleoclimate information from them. In contrast, speleothems dominated by matrix flowpaths and simple fracture structures are likely to be more suitable. These can be identified where drip monitoring exists or using approaches similar to ref. 41 to identify fractures by way of stalactite distribution on the cave ceiling. Where duplicated records from the same karst/climate region exist, a comparison of these records could result in a more complete

reconstruction of the hydroclimate drivers, rather than excluding records that don't agree.

Implications for quantified hydroclimate reconstructions. The Golgotha Cave case study demonstrates that the differences between coeval speleothem $\delta^{18}\text{O}$ records from the same cave can be controlled by the influence of the karst architecture (recharge thresholds, physical flowpaths) that results in dripwater $\delta^{18}\text{O}$ that departs from rainfall $\delta^{18}\text{O}$ that is in turn inherited by the speleothem. The global meta-analysis reveals that such within cave isotopic variability is common worldwide and is present in both dripwater and in replicated speleothem records across all time-scales and is independent of hydroclimate, host rock geology, cave depth or cave microclimate instability. A previous global meta-analysis of monitored cave datasets showed that dripwater $\delta^{18}\text{O}$ values were typically lower than precipitation-weighted mean annual rainfall $\delta^{18}\text{O}$ at warmer locations³⁷. Our expanded global study demonstrates that the additional impacts of flowpaths on within-cave isotopic variability are important over all climate types and karst characteristics.

Within-cave isotopic variability attributable to physical flowpath properties has been identified previously in cave monitoring studies^{59–61} and proxy system models^{15,62} have been used to simulate how flowpath variability can impact dripwater and speleothem $\delta^{18}\text{O}$. However, the outcome of these studies could be viewed as specific to a particular site or time domain. The novelty of our study is that we have utilised large global databases to demonstrate that within-cave variability in speleothem mean $\delta^{18}\text{O}$ values is ubiquitous. While we have not investigated isotopic fractionation during calcite precipitation in the SISALv2 data beyond demonstrating that there is no relationship between speleothem replication and distance from the cave entrance (an indication of cave microclimate instability), the results of our study supports that within-cave variability in speleothem mean $\delta^{18}\text{O}$ values may be accounted for by to within-cave variability in dripwater. Examination of other factors in the global meta-data analysis confirms the most parsimonious mechanism is the impact of flowpath characteristics—recharge threshold and fracture contribution of individual flowpaths—and we have captured this process in our case study.

Golgotha Cave hydrology experiences matrix flow through the highly porous Pleistocene aeolinite host rock³⁸. Globally, most karst is older and retains little or no primary porosity, hence

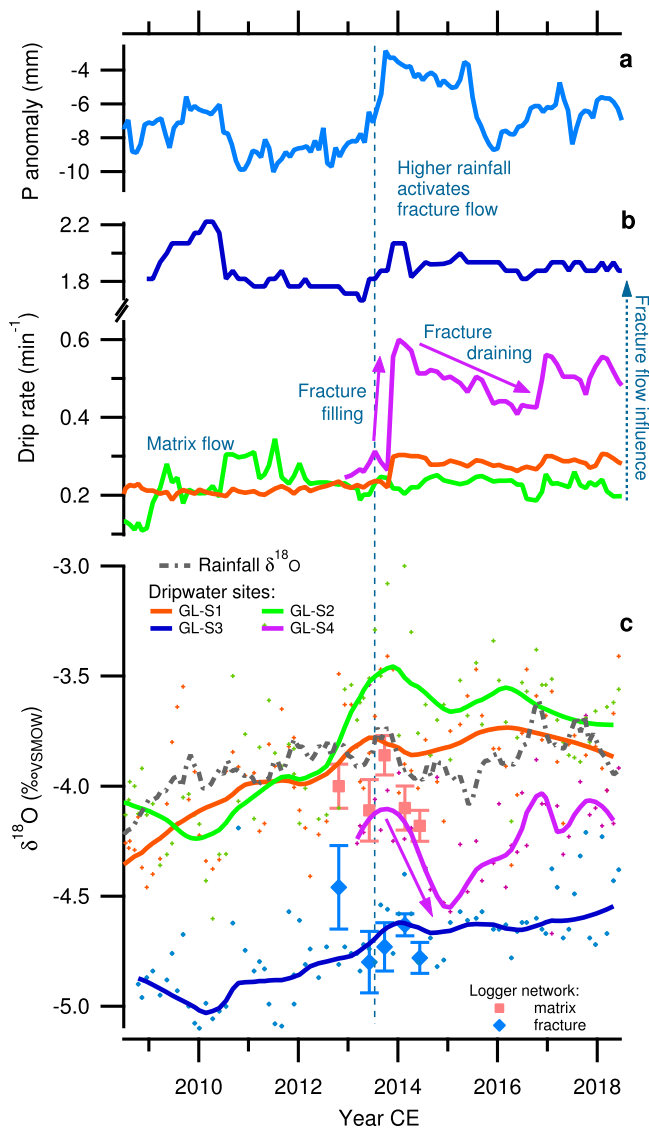


Fig. 5 Golgotha Cave monitoring data. **a** Smoothed monthly meteoric precipitation (P) anomalies (cerulean blue). **b** Monitored drip rates for speleothem sites GL-S1 (red), GL-S2 (green), GL-S3 (navy blue) and GL-S4 (purple). **c** Smoothed precipitation-weighted monthly rainfall $\delta^{18}\text{O}$ (grey dash) and smoothed dripwater $\delta^{18}\text{O}$ for drip sites where speleothems were collected (colours as for drip rates); mean $\delta^{18}\text{O}$ values of matrix (orange squares) and fracture flow sites (blue diamonds) in the drip logger array sampled during five field campaigns. Error bars represent $\pm 1\sigma$ of measurements from multiple sites. Monthly precipitation anomalies were calculated using the monthly climatological means from 1950 to 2020. An exponentially-weighted moving average (EWMA) was applied to monthly P anomalies with a half-life parameter of 36.6 months; similarly an EWMA was applied to monthly rainfall $\delta^{18}\text{O}$ using a 25 month half-life, as well as a lag of 19 months supported by our field studies in refs. 40,51. Dripwater $\delta^{18}\text{O}$ were smoothed with a loess 2nd order filter (span 0.3). Drip rates exhibit a threshold response to higher infiltration indicating the relative influence of fractures on each flowpath⁴⁰. For example, the drip for GL-S4 rapidly increases in response to higher precipitation anomalies during 2013 compared to the much smaller rise in the drip rate for GL-S1, indicating that a larger fracture component is feeding GL-S4. Over the same period, mean drip rate of the logger array increased from 0.16 ± 0.02 to 0.20 ± 0.40 for matrix flow sites and from 2.21 ± 0.40 to 8.32 ± 3.43 for fracture flow sites. The relative contribution of fracture flow to each drip site is inversely related to drip $\delta^{18}\text{O}$ values with activation of fractures occurring during periods of higher infiltration associated with lower rainfall $\delta^{18}\text{O}$ values.

water movement is likely to be more impacted by heterogeneities in flowpaths through fractures. In mature limestones, a high density of fissures, sediment-filled structures and paleokarst could similarly act as porous media; and drips with matrix flow properties have been identified in many monitored caves from mature limestones (e.g. refs. 27,60,61).

Fractures and their activation thresholds result in a bias of the contribution of rainfall events to different flowpaths giving rise to drip sites with different mean $\delta^{18}\text{O}$ values. Speleothems with a larger fracture contribution to their flowpath will likely have a mean value that is further from precipitation-weighted mean annual rainfall $\delta^{18}\text{O}$. This has implications for using speleothems as isotopic targets for assessing the performance of climate models, e.g., ref. 13. Calibrated karst proxy system models⁶² would allow for the possibility of reconstructing mean precipitation $\delta^{18}\text{O}$, which is directly comparable to output from isotope-enabled general circulation models¹³. This highlights the importance of developing proxy system models that represent karst processes.

Our findings that the relative contribution of fracture versus matrix flow impacts dripwater and speleothem $\delta^{18}\text{O}$ also has important implications for the interpretation of speleothem $\delta^{18}\text{O}$ within an individual record. Larger contributions from fracture flow are activated during periods of higher rainfall. This amplifies the non-linear relationship between rainfall and speleothem $\delta^{18}\text{O}$ as shown in our case study. A quantified reconstruction of past rainfall from Golgotha Cave speleothems requires a calibrated proxy system model able to reconcile the within-cave variability in $\delta^{18}\text{O}$ arising from matrix versus fracture flow and is an objective for a forthcoming study. For other studies, we highlight that the implications of our findings suggest that variability within speleothem $\delta^{18}\text{O}$ can be larger than what can be attributed to direct changes in rainfall $\delta^{18}\text{O}$ and this should be considered whether applied to last millennia climate reconstructions or to assessing glacial–interglacial transitions in older speleothems.

Methods

Global meta-analysis. The dataset of ref. 37 was extended to include studies with at least quarterly dripwater sampling over 12 months and to include additional sites that had been rejected by ref. 37 on the basis of not having nearby rainfall $\delta^{18}\text{O}$ data. Mean $\delta^{18}\text{O}$ for each drip site over a 12 month period was calculated and the range of these mean values for each cave was determined (Supplementary Data 1). For speleothem data, we utilised the SISALv2 database^{10,11,13} to identify caves with coeval speleothem $\delta^{18}\text{O}$ records satisfying the following criteria, coded in R package v1.0.7., `mineralogy = calcite AND coeval interval exceeds 10% of the minimum age of overlap AND overlap interval exceeds twice the age uncertainty linearly extrapolated beyond the maximum age AND twice the age uncertainty linearly extrapolated less than the minimum age AND each section contain >10 $\delta^{18}\text{O}$ measurements`. We used the chronologies as they appear in SISALv2. The mean $\delta^{18}\text{O}$ value for each speleothem record was calculated for the duration of replication and difference between the means calculated ($\Delta\delta^{18}\text{O}_{\text{means}}$) for each pair of coeval records (Supplementary Data 2 and 3). If a hiatus was entered in SISALv2 within the period of coeval growth, data were omitted from the other record over this interval before calculating the mean of each speleothem record. For $\Delta\delta^{18}\text{O}_{\text{means}} > 0.5\text{‰}$ a plot of the SISALv2 data (not shown) for each coeval pair and their mean values was generated to visually check if hiatuses were identified. In one case (entity ID 487) it was apparent that the mean value was impacted by a hiatus not identified in SISALv2 and this record was removed from our analysis. Additionally, where data from the same speleothem appears in SISALv2 as separate entities owing to revised records in different publications, the entity with the longer record (time span) was used. If the growth interval was the same, the entity with the higher resolution record was used. We assessed the robustness of our approach by examining the impact of varying the criteria (Supplementary Table 1). Cave meta-data were extracted from SISALv2¹¹ and climate variables from WorldClim V1,⁶³ the latter use 1960–1990 as the period for climatology. Aridity index was calculated as precipitation divided by actual evapotranspiration, WorldClim V1 products, Bio4 and Bio15, were used as seasonality indices for temperature and precipitation, respectively. Cave depth and distance to entrance data were not available for all sites. In cases where elevation data were not provided, these were taken from ref. 64. Mean depth is the estimated mean thickness of host rock above site of dripwater monitoring or collected speleothem.

Table 1 Farmed calcite and dripwater $\delta^{18}\text{O}$ data.

Date range (MM/YY)	Drip site	Mean calcite $\delta^{18}\text{O}$ (‰ vPDB) ^a	Mean water $\delta^{18}\text{O}$ (‰ vSMOW) ^{a,b}	$\alpha_{\text{calcite-water}}$	1000ln $\alpha_{\text{calcite-water}}$ (‰)
10/08–04/11	1A	-3.27 ± 0.09 (3)	-4.04 ± 0.07 (21)	1.03172 ± 0.00003	31.22 ± 0.03
06/16–10/17	1A	-2.88 ± 0.01 (2)	-3.80 ± 0.03 (14)	1.03188 ± 0.00001	31.38 ± 0.01
06/16–10/17	1IV	-3.47 ± 0.02 (2)	-4.16 ± 0.06 (14)	1.03163 ± 0.00002	31.14 ± 0.02
10/08–04/11	2B	-3.09 ± 0.10 (2)	-4.09 ± 0.11 (20)	1.03195 ± 0.00004	31.45 ± 0.04
05/11–12/11	2B	-2.90 ± 0.10 (2)	-3.88 ± 0.03 (6)	1.03193 ± 0.00004	31.43 ± 0.04
10/08–04/11	2E	-3.86 ± 0.10 (2)	-4.88 ± 0.04 (22)	1.03197 ± 0.00003	31.47 ± 0.03
05/11–12/11	2E	-3.80 ± 0.19 (2)	-4.83 ± 0.03 (6)	1.03198 ± 0.00005	31.48 ± 0.05
01/12–10/12	2E	-3.82 ± 0.13 (3)	-4.79 ± 0.02 (5)	1.03193 ± 0.00004	31.43 ± 0.03
06/16–10/17	2E	-3.80 ± 0.30 (2)	-4.56 ± 0.05 (14)	1.03170 ± 0.00008	31.21 ± 0.08
Empirical bulk fractionation factor for Golgotha Cave ($n = 9$)				1.03185 ± 0.00013	31.36 ± 0.13

Mean $\delta^{18}\text{O}$ values for farmed calcites and corresponding dripwater collected at each site between 2008–2017. The calculated fractionation factor between calcite and water is shown for each interval, as well as an overall mean value calculated (termed the empirical bulk fractionation factor).

^a ± 1 standard deviation; value in brackets indicates number of observations.

^bCalculated using numerically smoothed values as for Fig. 5c.

Golgotha Cave dripwater and rainfall data. Data presented here are an extension of published³⁸ drip and rainfall $\delta^{18}\text{O}$ data plus new dripwater data collected at the site of speleothem GL-S4 (2012–2019) as well as additional samples collected over 2–5 days durations from the automated logger array during five separate field campaigns. Methods for drip and rainfall $\delta^{18}\text{O}$ appear in ref. 38 with the exception of $\delta^{18}\text{O}$ measurements being made using Picarro L2120-I Water Analyser at ANSTO (see ref. 65 for method) from 2012 onwards. Supplementary Table 3 contains identification codes for dripwater and speleothem pairing and summarises site data. To estimate the impact of the 1970s rainfall decrease on rainfall $\delta^{18}\text{O}$, the rainfall $\delta^{18}\text{O}$ -amount relationship determined for Golgotha Cave (based on daily rainfall sampling between 2005–2018) of ref. 52 was applied to the daily rainfall data from the nearest Australian Bureau of Meteorology station (station ID 9547; record began 1926), <4 km from Golgotha Cave. Mean values were compared between 1926–1969 and 1970–2018.

Stalagmite stable isotopes. Stalagmites were collected under scientific license CE003472 issued by Western Australia's Department of Biodiversity, Conservation and Attractions. Each speleothem was milled along the growth axis using a Taig micromill to produce homogenised powders representing increments of 0.1–0.2 mm, depending on the speleothem growth rate. Powders were weighed to 180–220 μg and analysed for $\delta^{18}\text{O}$ and $\delta^{13}\text{C}$ using a Finnigan MAT-251 isotope ratio mass spectrometer coupled to a Kiel I carbonate device, or a Thermo MAT-253 isotope ratio mass spectrometer coupled to a Kiel IV carbonate device (using 110–130 μg samples), at the Research School of Earth Sciences, ANU. Analyses were calibrated using NBS-19 standard ($\delta^{18}\text{O}_{\text{v-PDB}} = -2.20\text{‰}$ and $\delta^{13}\text{C}_{\text{v-PDB}} = 1.95\text{‰}$). A further linear correction for $\delta^{18}\text{O}$ measurements was carried out using the NBS-18 standard ($\delta^{18}\text{O}_{\text{v-PDB}} = -23.0\text{‰}$). The original delta values for NBS-19 and NBS-18 are used to maintain consistency of results through time in the RSES Stable Isotope Facility. Analytical precision for the analyses reported here (NBS-19) are $\pm 0.04\text{‰}$ for $\delta^{18}\text{O}$ and $\pm 0.02\text{‰}$ for $\delta^{13}\text{C}$ ($N = 236$) for the MAT-251; and $\pm 0.05\text{‰}$ for $\delta^{18}\text{O}$ and $\pm 0.01\text{‰}$ ($N = 27$) for the MAT-253 instrument ($\pm 1\sigma$ standard deviation).

Speleothem chronologies. Speleothem chronologies were determined by combining information from the date of collection, bomb pulse chronology⁶⁶, laminae counting of annual Sr concentration and U-series disequilibrium (see Supplementary Table 4 for further information). U-Th age measurements followed the method of ref. 67. Briefly, calcite wafers weighing 100–200 mg were dissolved and equilibrated with a mixed ^{229}Th – ^{233}U – ^{236}U tracer before U and Th are extracted in a single solution using Eichrom TRU resin before measurement on a Nu Plasma multicollector ICPMS where isotope ratios of both elements are measured simultaneously. A ratio of initial [$^{230}\text{Th}/^{232}\text{Th}$] = 0.33 ± 0.25 was applied and is defined by modelling the ratio required to bring ages into age-depth order for each stalagmite. This ratio is further supported by comparing the U/Th ADM to the laminae chronology for stalagmite GL-S4. Data for age measurements are given in Supplementary Data 5.

X-ray fluorescence microscopy (XFM) maps of Sr concentration were acquired on the speleothem polished slabs at 2 μm resolution (pixel size) at the XFM beamline at the Australian Synchrotron⁶⁸ using a monochromatic incident energy of 18.5 keV focussed to spot size of 1.5 μm , and dwell per pixel from 1 to 4 ms. The XFM elemental maps were created and analysed using GeoPIXE software, quantified by using single element Mn, Fe and Pt foils (Micromatter, Canada) and corrected by using a Ca matrix factor. Laminae counting and error estimate was made by determining the position of the Sr peaks on two parallel areas of the Sr

maps at three confidence levels (>95, 50–95 and <50% confidence) using ImageJ software package according to the method outlined in ref. 69.

Data availability

The SISAL (Speleothem Isotopes Synthesis and Analysis Working Group) database version 2, that supports Figs. 1 and 2, Supplementary Figs. 1 and 2, is archived at The University of Reading <https://researchdata.reading.ac.uk/256/>. The Golgotha Cave speleothem and drip water time series data are archived on the PANGEA paleoclimate data repository (<https://www.pangaea.de/>) under data submission identifiers PDI-30276 (titled: Golgotha Cave dripwater isotopes) and PDI-30277 (titled: Golgotha Cave stalagmite records 1 ka).

Received: 9 August 2021; Accepted: 17 January 2022;

Published online: 15 February 2022

References

- Dansgaard, W. Stable isotopes in precipitation. *Tellus* **4**, 436–468 (1964).
- Gat, J. R. Atmospheric water balance—the isotopic perspective. *Hydrol. Process.* **14**, 1357–1369 (2000).
- Brady, E. et al. The connected isotopic water cycle in the community earth system model version 1. *J. Adv. Model. Earth Syst.* **11**, 2547–2566 (2019).
- Petit, J. R. et al. Climatic and atmospheric history of the past 420,000 years from the Vostok ice core, Antarctica. *Nature* **399**, 429–436 (1999).
- Liu, Z. et al. Evolution and forcing mechanisms of El Niño over the past 21,000 years. *Nature* **515**, 550–553 (2014).
- Clark, P. U. et al. Oceanic forcing of penultimate deglacial and last interglacial sea-level rise. *Nature* **577**, 660–664 (2020).
- Cheng, H. et al. The Asian monsoon over the past 640,000 years and ice age terminations. *Nature* **534**, 640–646 (2016).
- Partin, J. W., Cobb, K. M., Adkins, J. F., Clark, B. & Fernandez, D. P. Millennial-scale trends in west Pacific warm pool hydrology since the last Glacial maximum. *Nature* **449**, 452–456 (2007).
- Bolliet, T. et al. Water and carbon stable isotope records from natural archives: a new database and interactive online platform for data browsing, visualizing and downloading. *Clim. Past* **12**, 1693–1719 (2016).
- Atsawawanunt, K. et al. The SISAL database: a global resource to document oxygen and carbon isotope records from speleothems. *Earth Syst. Sci. Data* **10**, 1687–1713 (2018).
- Comas-Bru, L. et al. SISALv2: a comprehensive speleothem isotope database with multiple age-depth models. *Earth Syst. Sci. Data* **12**, 2579–2606 (2020).
- Comas-Bru, L. & Harrison, S. Bringing added value to speleothem research. *Quaternary* **2**, 7 (2019).
- Comas-Bru, L. et al. Evaluating model outputs using integrated global speleothem records of climate change since the last glacial. *Clim. Past* **15**, 1557–1579 (2019).
- Hendy, C. The isotope geochemistry of speleothems-I. The calculation of the effects of different modes of formation on the isotopic composition of speleothems and their applicability as palaeoclimatic indicators. *Geochim. Cosmochim. Acta* **35**, 802–824 (1971).
- Bradley, C., Baker, A., Jex, C. N. & Leng, M. J. Hydrological uncertainties in the modelling of cave drip-water $\delta^{18}\text{O}$ and the implications for stalagmite palaeoclimate reconstructions. *Quat. Sci. Rev.* **29**, 2201–2214 (2010).

16. Mickler, P. J., Stern, L. A. & Banner, J. L. Large kinetic isotope effects in modern speleothems. *Geol. Soc. Am. Bull.* **118**, 65–81 (2006).
17. Hansen, M., Scholz, D., Schöne, B. R. & Spötl, C. Simulating speleothem growth in the laboratory: Determination of the stable isotope fractionation ($\delta^{13}\text{C}$ and $\delta^{18}\text{O}$) between H_2O , DIC and CaCO_3 . *Chem. Geol.* **509**, 20–44 (2019).
18. Guo, W. & Zhou, C. Patterns and controls of disequilibrium isotope effects in speleothems: insights from an isotope-enabled diffusion-reaction model and implications for quantitative thermometry. *Geochim. Cosmochim. Acta* **267**, 196–226 (2019).
19. Deininger, M. et al. Are oxygen isotope fractionation factors between calcite and water derived from speleothems systematically biased due to prior calcite precipitation (PCP)? *Geochim. Cosmochim. Acta* **305**, 212–227 (2021).
20. Baker, A. & Bradley, C. Modern stalagmite $\delta^{18}\text{O}$: instrumental calibration and forward modelling. *Glob. Planet. Change* **71**, 201–206 (2010).
21. Jex, C. N., Phipps, S. J., Baker, A. & Bradley, C. Reducing uncertainty in the climatic interpretations of speleothem $\delta^{18}\text{O}$. *Geophys. Res. Lett.* **40**, 2259–2264 (2013).
22. Bar-Mathews, M., Ayalon, A., Kaufman, A. & Wasserburg, G. J. The Eastern Mediterranean paleoclimate as a reflection of regional events: Soreq cave, Israel. *Earth Planet. Sci. Lett.* **166**, 85–95 (1999).
23. Spötl, C., Fairchild, I. J. & Tooth, A. F. Cave air control on dripwater geochemistry, Obir Caves (Austria): Implications for speleothem deposition in dynamically ventilated caves. *Geochim. Cosmochim. Acta* **69**, 2451–2468 (2005).
24. Matthey, D. et al. A 53 year seasonally resolved oxygen and carbon isotope record from a modern Gibraltar speleothem: reconstructed drip water and relationship to local precipitation. *Earth Planet. Sci. Lett.* **269**, 80–95 (2008).
25. Tremaine, D. M., Froelich, P. N. & Wang, Y. Speleothem calcite formed in situ: modern calibration of $\delta^{18}\text{O}$ and $\delta^{13}\text{C}$ paleoclimate proxies in a continuously-monitored natural cave system. *Geochim. Cosmochim. Acta* **75**, 4929–4950 (2011).
26. Riechelmann, D. F. C. et al. Monitoring Bunker Cave (NW Germany): a prerequisite to interpret geochemical proxy data of speleothems from this site. *J. Hydrol.* **409**, 682–695 (2011).
27. Pape, J. R., Banner, J. L., Mack, L. E., Musgrove, M. & Guilfoyle, A. Controls on oxygen isotope variability in precipitation and cave drip waters, central Texas, USA. *J. Hydrol.* **385**, 203–215 (2010).
28. Dorale, J. A. & Liu, Z. H. Limitations of Hendy Test criteria in judging the paleoclimatic suitability of speleothems and the need for replication. *J. Cave Karst Stud.* **71**, 73–80 (2009).
29. Fohlmeister, J. et al. Bunker Cave stalagmites: an archive for central European Holocene climate variability. *Clim. Past* **8**, 1751–1764 (2012).
30. Cai, Y. et al. Variability of stalagmite-inferred Indian monsoon precipitation over the past 252,000 y. *Proc. Natl Acad. Sci.* **112**, 2954 (2015).
31. Lachniet, M. S. Climatic and environmental controls on speleothem oxygen isotope values. *Quat. Sci. Rev.* **28**, 412–432 (2009).
32. Carolin, S. A. et al. Varied response of Western Pacific hydrology to climate forcings over the last Glacial period. *Science* **340**, 1564–1566 (2013).
33. Williams, P. W., King, D. N. T., Zhao, J. X. & Collerson, K. D. Speleothem master chronologies: combined holocene O-18 and C-13 records from the North Island of New Zealand and their palaeoenvironmental interpretation. *Holocene* **14**, 194–208 (2004).
34. Ayliffe, L. K. et al. Rapid interhemispheric climate links via the Australasian monsoon during the last deglaciation. *Nat. Commun.* **4**, 2908 (2013).
35. Caley, T., Roche, D. M., Waelbroeck, C. & Michel, E. Oxygen stable isotopes during the last Glacial maximum climate: perspectives from data model (iLOVECLIM) comparison. *Clim. Past* **10**, 1939–1955 (2014).
36. Hartmann, A. & Baker, A. Modelling karst vadose zone hydrology and its relevance for paleoclimate reconstruction. *Earth Sci. Rev.* **172**, 178–192 (2017).
37. Baker, A. et al. Global analysis reveals climatic controls on the oxygen isotope composition of cave drip water. *Nat. Commun.* **10**, 2984 (2019).
38. Treble, P. C. et al. An isotopic and modelling study of flow paths and storage in Quaternary calcarenite, SW Australia; implications for speleothem paleoclimate records. *Quat. Sci. Rev.* **64**, 90–103 (2013).
39. Mahmud, K., Mariethoz, G., Baker, A. & Treble, P. C. Hydrological characterization of cave drip waters in a porous limestone: Golgotha Cave, Western Australia. *Hydrol. Earth Syst. Sci.* **22**, 977–988 (2018).
40. Mahmud, K. et al. Estimation of deep infiltration in unsaturated limestone environments using cave LiDAR and drip count data. *Hydrol. Earth Syst. Sci.* **20**, 359–373 (2016).
41. Mahmud, K., Mariethoz, G., Treble, P. C. & Baker, A. Terrestrial LiDAR survey and morphological analysis to identify infiltration properties in the Tamala Limestone, Western Australia. *IEEE J. Sel. Topics Appl. Earth Observ. Remote Sens.* **8**, 4871–4881 (2015).
42. Ostermann, D. R. & Curry, W. B. Calibration of stable isotopic data: an enriched $\delta^{18}\text{O}$ standard used for source gas mixing detection and correction. *Paleoceanography* **15**, 353–360 (2000).
43. Wassenaar, L. I. et al. Seeking excellence: an evaluation of 235 international laboratories conducting water isotope analyses by isotope-ratio and laser-absorption spectrometry. *Rapid Commun. Mass Spectrom.* **32**, 393–406, (2018).
44. Boch, R. *Stalagmites from Katerloch Cave, Austria: Growth dynamics and high-resolution records of climate change*. PhD thesis, (Leopold-Franzens-Universität Innsbruck, 2008).
45. Baker, A. & Bradley, C. Modern stalagmite $\delta^{18}\text{O}$: instrumental calibration and forward modelling. *Glob. Planet. Change* **71**, 201–206 (2011).
46. Fuller, L. et al. Isotope hydrology of dripwaters in a Scottish cave and implications for stalagmite palaeoclimate research. *Hydrol. Earth Syst. Sci.* **12**, 1065–1074 (2008).
47. Moreno, A. et al. New speleothem data from Molinos and Ejulve caves reveal Holocene hydrological variability in northeast Iberia. *Quat. Res.* **88**, 223–233 (2017).
48. Riechelmann, S. et al. Sensitivity of Bunker Cave to climatic forcings highlighted through multi-annual monitoring of rain-, soil-, and dripwaters. *Chem. Geol.* **449**, 194–205 (2017).
49. Moreno, A. et al. Climate controls on rainfall isotopes and their effects on cave drip water and speleothem growth: the case of Molinos cave (Teruel, NE Spain). *Clim. Dyn.* **43**, 221–241 (2014).
50. Duan, W. et al. The transfer of seasonal isotopic variability between precipitation and drip water at eight caves in the monsoon region of China. *Geochim. Cosmochim. Acta* **183**, 250–266 (2016).
51. Leopold, M., Gupanis-Broadway, C., Baker, A., Hankin, S. & Treble, P. Time lapse electric resistivity tomography to portray infiltration and hydrologic flow paths from surface to cave. *J. Hydrol.* **593**, 125810 (2021).
52. Griffiths, A. D., Treble, P., Hope, P. & Rudeva, I. Rainfall stable water isotope variability in coastal southwestern Western Australia and its relationship to climate on multiple timescales. *Journal of Geophysical Research: Atmospheres*, **127**, e2021JD035433. <https://doi.org/10.1029/2021JD035433> (2022).
53. Lachniet, M. S. Climatic and environmental controls on speleothem oxygen-isotope values. *Quat. Sci. Rev.* **28**, 412–432 (2009).
54. Fairchild, I. J. et al. Controls on trace element (Sr-Mg) compositions of carbonate cave waters: implications for speleothem climatic records. *Chem. Geol.* **166**, 255–269 (2000).
55. Fischer, M. J. & Treble, P. C. Calibrating climate $\delta^{18}\text{O}$ regression models for the interpretation of high-resolution speleothem $\delta^{18}\text{O}$ time series. *J. Geophys. Res. Atmos.* **113**, D17103 (2008).
56. Ireson, A. M., Butler, A. B. & Wheeler, H. S. Evidence for the onset and persistence with depth of preferential flow in unsaturated fractured porous media. *Hydrol. Res.* **43**, 707–719 (2012).
57. Hope, P., Timbal, B. & Fawcett, R. Associations between rainfall variability in the southwest and southeast of Australia and their evolution through time. *Int. J. Climatol.* **30**, 1360–1371 (2010).
58. Mühlinghaus, C., Scholz, D. & Mangini, A. Modelling fractionation of stable isotopes in stalagmites. *Geochim. Cosmochim. Acta* **73**, 7275–7289 (2009).
59. Chapman, J. B., Ingraham, N. L. & Hess, J. W. Isotopic investigation of infiltration and unsaturated zone flow processes at Carlsbad Cavern, New Mexico. *J. Hydrol.* **133**, 343–363 (1992).
60. Ayalon, A., Bar-Mathews, M. & Sass, E. Rainfall-recharge relationships within a karstic terrain within the Eastern Mediterranean semi-arid region, Israel: $\delta^{18}\text{O}$ and δD characteristics. *J. Hydrol.* **207**, 18–30 (1998).
61. Nava-Fernandez, C. et al. Pacific climate reflected in Waipuna Cave drip water hydrochemistry. *Hydrol. Earth Syst. Sci.* **24**, 3361–3380 (2020).
62. Hu, J. et al. Assessing proxy system models of cave dripwater $\delta^{18}\text{O}$ variability. *Quat. Sci. Rev.* **254**, 106799 (2021).
63. Hijmans, R. J. et al. The WorldClim interpolated global terrestrial climate surfaces, version 1.3. www.biogeography.berkeley.edu. (2004).
64. Spötl, C., Moseley, G., Johnson, K., Matthey, D. & Treble, P. Cave monitoring database. www.cave-monitoring.org. (2020).
65. Crawford, J., Hollins, S. E., Meredith, K. T. & Hughes, C. E. Precipitation stable isotope variability and subcloud evaporation processes in a semi-arid region. *Hydrol. Process.* **31**, 20–34 (2017).
66. Markowska, M. et al. Modelling the ^{14}C bomb-pulse in young speleothems using a soil carbon continuum model. *Geochim. Cosmochim. Acta* **261**, 342–367 (2019).
67. Hellstrom, J. Rapid and accurate U/Th dating using parallel ion-counting multi-collector ICP-MS. *J. Anal. Atomic Spectrom.* **18**, 1346–1351 (2003).
68. Howard, D. L. et al. The XFM beamline at the Australian synchrotron. *J. Synchrotron Radiat.* **27**, 1447–1458 (2020).
69. Faraji, M. et al. Accurate dating of stalagmites from low seasonal contrast tropical Pacific climate using Sr 2D maps, fabrics and annual hydrological cycles. *Sci. Rep.* **11**, 2178 (2021).
70. BGR, IAH, KIT & UNESCO. *World Karst Aquifer Map*. (WHYMAP, BGR, 2017).

Acknowledgements

This research is supported by funding from the Australian Research Council (DP140102059 to PCT and NJA) and a Land & Water Australia grant (ANU52). The

micro-XRF analysis research was undertaken on the X-ray fluorescence microscopy (XFM) beamline at the Australian Synchrotron, part of ANSTO under proposals PA13457 and PA14312. We used the SISALv2 database, made possible through the Speleothem Isotope Synthesis and Analysis (SISAL) working group of the Past Global Changes (PAGES) project, supported by the Swiss Academy of Sciences and the Chinese Academy of Sciences. We gratefully acknowledge the assistance from the staff at Calgardup Caves (Department of Biodiversity, Conservations and Attractions) to conduct the cave monitoring, as well as Ian Fairchild for comments on the manuscript, Fabio Oriani for assistance with image processing of synchrotron maps and technical support from Barbora Gallagher, Jennifer van Holst, Joe Cali, Joan Cowley, Heather Scott-Gagan, Jennifer Wurtzel and Lewis Adler.

Author contributions

This manuscript was devised and written by PCT with input from A.Baker and A.D.G. All co-authors contributed to the writing of the paper. Golgotha Cave speleothem and monitoring data were created by PCT with input from N.J.A., J.C.H., J.C., M.K.G., A.Borsato, P.B., M.M., D.J.P., and A.Baker. A.Baker, P.C.T., J.C., S.C.P., and S.H. conducted the analysis for Fig. 1.

Competing interests

The authors declare no competing interests.

Additional information

Supplementary information The online version contains supplementary material available at <https://doi.org/10.1038/s43247-022-00347-3>.

Correspondence and requests for materials should be addressed to Pauline C. Treble.

Peer review information *Communications Earth & Environment* thanks Jasper Wassenburg and the other, anonymous, reviewer(s) for their contribution to the peer review of this work. Primary Handling Editors: Joe Aslin, Heike Langenberg. Peer reviewer reports are available.

Reprints and permission information is available at <http://www.nature.com/reprints>

Publisher's note Springer Nature remains neutral with regard to jurisdictional claims in published maps and institutional affiliations.



Open Access This article is licensed under a Creative Commons Attribution 4.0 International License, which permits use, sharing, adaptation, distribution and reproduction in any medium or format, as long as you give appropriate credit to the original author(s) and the source, provide a link to the Creative Commons license, and indicate if changes were made. The images or other third party material in this article are included in the article's Creative Commons license, unless indicated otherwise in a credit line to the material. If material is not included in the article's Creative Commons license and your intended use is not permitted by statutory regulation or exceeds the permitted use, you will need to obtain permission directly from the copyright holder. To view a copy of this license, visit <http://creativecommons.org/licenses/by/4.0/>.

© Crown 2022